Published in final edited form as:
Geophys Res Lett. 2017 November 28; 44(22): 11248–11256. doi:10.1002/2017GL075431.

Ion Densities in the Nightside Ionosphere of Mars: Effects of Electron Impact Ionization

Z. Girazian[1], **P. Mahaffy**[1], **R. J. Lillis**[2], **M. Benna**[1,3], **M. Elrod**[1,4], **C. M. Fowler**[5], and **D. L. Mitchell**[2]

[1]NASA Goddard Space Flight Center, Greenbelt, Maryland, USA

[2]Space Sciences Laboratory, University of California, Berkeley, California, USA

[3]CRESST, University of Maryland Baltimore County, Baltimore, Maryland, USA

[4]CRESST, University of Maryland, College Park, Maryland, USA

[5]Laboratory for Atmospheric and Space Physics, University of Colorado Boulder, Boulder, Colorado, USA

Abstract

We use observations from the Mars Atmosphere and Volatile EvolutioN(MAVEN) mission to show how superthermal electron fluxes and crustal magnetic fields affect ion densities in the nightside ionosphere of Mars. We find that, due to electron impact ionization, high electron fluxes significantly increase the CO_2^+, O^+, and O_2^+ densities below 200 km, but only modestly increase the NO^+ density. High electron fluxes also produce distinct peaks in the CO_2^+, O^+, and O_2^+ altitude profiles. We also find that superthermal electron fluxes are smaller near strong crustal magnetic fields. Consequently, nightside ion densities are also smaller near strong crustal fields because they decay without being replenished by electron impact ionization. Furthermore, the NO^+/O_2^+ ratio is enhanced near strong crustal fields because, in the absence of electron impact ionization, O_2^+ is converted into NO^+ and not replenished. Our results show that electron impact ionization is a significant source of CO_2^+, O^+, and O_2^+ in the nightside ionosphere of Mars.

1. Introduction

In the nightside ionosphere of Mars, electron densities are patchy, variable, and controlled largely by the strength and topology of crustal magnetic fields. Observed peak electron densities vary between 10^3 and 5×10^4 cm^{-3}, but are often too small ($<5 \times 10^3$ cm^{-3}) to be detected by remote sensing instruments *[Zhang et al.,* 1990; *Němec et al.,* 2010, 2011; *Withers et al.,* 2012; *Diéval et al.,* 2014; *Fowler et al.,* 2015]. The largest peak densities are found near vertical crustal fields, which form cusps that allow superthermal electrons to precipitate into the atmosphere. In contrast, smaller peak densities are found near horizontal

Z. Girazian, zachary.r.girazian@nasa.gov.

crustal fields, which prevent superthermal electrons from precipitating into the atmosphere *[Mitchell et al.,* 2001; *Brain et al.,* 2007; *Safaeinili et al.,* 2007; *Gurnett et al.,* 2008; *Němec et al.,* 2010, 2011; *Dubinin et al.,* 2016; *Lillis and Brain*, 2013; *Shane et al.,* 2016]. These findings have led to the conclusion that electron impact ionization plays an important role in forming the nightside ionosphere of Mars.

This conclusion has been supported by electron precipitation models, which predict peak electron densities and peak altitudes (120–180 km) that are consistent with nightside observations *[Haider et al.,* 1992; *Fillingim et al.,* 2007, 2010; *Lillis et al.,* 2009, 2011], and shown that the strength and topology of crustal fields control electron impact ionization rates *[Lillis and Fang*, 2015]. Precipitation models also predict that electron impact ionization will affect the chemical composition of the nightside ionosphere [*Fox et al.,* 1993; *Haider*, 1997; *Haider et al.,* 2013]. This, however, has not been confirmed by observations because nightside data has historically been limited to measurements of the electron density and total electron content [e.g., *Zhang et al.,* 1990; *Withers et al.,* 2012;*Dubinin et al.,* 2016]. With new data from the Mars Atmosphere and Volatile EvolutioN (MAVEN) mission *[Jakosky et al.,* 2015a, b], we can now address this issue.

MAVEN is equipped with instruments that measure ion densities, superthermal electron fluxes, and magnetic fields in the nightside ionosphere. Here we use a two month period of these observations during which MAVEN was in the southern hemisphere of Mars, and the instruments sampled locations where there are both strong and weak crustal magnetic fields. We use this data to show how nightside CO_2^+, O^+, O_2^+, and NO^+ densities vary with superthermal electron fluxes, and how they depend on the strength and topology of crustal magnetic fields.

2. MAVEN Data

2.1. Data Sources

We use data from three MAVEN instruments, all of which obtain in situ measurements along MAVEN's orbit. The Neutral Gas and Ion Mass Spectrometer (NGIMS) provides measurements of CO_2^+, O^+, O_2^+, and NO^+ densities *[Mahaffy et al.,* 2015a; *Benna et al.,* 2015a, b]; the MAVEN magnetometer (MAG) provides measurements of the vector magnetic field *[Connerney et al.,* 2015a, b]; and the Solar Wind Electron Analyzer (SWEA) provides measurements of omni-directional electron fluxes at logarithmically-spaced energies between 3 and 4600 eV *[Mitchell et al.,* 2016]. For NGIMS and MAG, we use the key parameter (KP) data products which have a 4-second time resolution. For SWEA, we use the Level 2 data products after interpolating them onto the same 4-second time grid as the NGIMS and MAG KP data.

2.2. Data Distribution

We use observations from 8 July through 16 September in 2015, during which Mars was approaching aphelion during northern hemisphere spring equinox (L_s=10°−42°). We use only the nightside observations from this period, when the solar zenith angle (SZA) was greater than 110° and the ionosphere was shadowed from solar EUV radiation. Figure 1(top

left) shows the geographic distribution of the observations in relation to the crustal magnetic field strength at 200 km *[Morschhauser et al.,* 2014]. The observations were obtained in the southern hemisphere at latitudes between −75° and −50° where there are strong crustal magnetic fields between 120° and 240° E. longitude. At longitudes outside this region the crustal fields are much weaker.

Figure 1 also shows the altitudes of the observations with respect to latitude, longitude, and SZA. The periapsis altitudes were typically around 145 km, but there was also a “deep dip” campaign that lowered the periapsis down to 120 km for several orbits. The latitudes varied between −75° and −50°, but were concentrated between −75° and −70° (top right panel). The observations were uniformly distributed in longitude allowing for even sampling of the strong and weak crustal field regions (bottom left panel).

The SZAs varied between 110° and 130°, but observations below 160 km only extended up to a SZA of 120° (bottom right panel). Although the observations were obtained at both the dawn and dusk terminators, inspection of the dawn and dusk data separately showed no major differences. We therefore make no distinction between the dawn and dusk data in our analysis.

3. Analysis

3.1. Observations During Two Periapsis Passes

Figure 2 shows the measured magnetic field, electron energy spectra, and ion densities during two MAVEN periapsis passes. The left column shows a pass in a weak crustal field region where the field strength was typically less than 20 nT. During this pass SWEA measured intermittent but extended periods of high electron fluxes (labeled A, B, C). These periods coincided with large increases in the NGIMS CO_2^+ and O^+ densities, presumably caused by electron impact ionization of CO_2 and O, which are the most abundant neutral species in the thermosphere [*Nier and McElroy*, 1977; *Mahaffy et al.,* 2015b]

The right column in Fig. 2 shows a periapsis pass in a strong crustal field region where the field strength exceeded 600 nT near periapsis. During this pass there were no extended periods of high SWEA electron fluxes in the strong crustal field region (at SZAs >114° and E. longitudes > 140°). Instead, there were narrow spikes of high electron flux confined to magnetic cusps where the field was predominately radial. These narrow spikes also coincided with sharp increases in the NGIMS ion densities.

Comparing the ion densities from the two passes (bottom two panels) shows that the CO_2^+, O^+, and O_2^+ densities were smaller during the second pass when electron fluxes were lower. This suggests that ions densities near strong crustal fields are smaller because they decay without being replenished by electron impact ionization. We will further analyze the effects of crustal fields in Section 3.4, but first we use the full data set to show how ion densities depend on superthermal electron fluxes.

3.2. Ion Densities as a Function of the Electron Flux

Although a direct calculation of the electron impact and chemical production rates of CO_2^+, O^+, O_2^+, and NO^+ would be beneficial, it is out of the scope of this paper. Calculating the ion production rates requires measurements of the CO_2, O, N, and NO neutral densities. NGIMS measurements of CO_2 and O, however, are only calibrated for the inbound portion of each periapsis pass and NGIMS measurements of N and NO are not yet calibrated. Since the neutral densities are unavailable, a detailed modeling study of electron impact ionization is reserved for a future study. Instead, we focus on analyzing the observations.

To show how nightside ion densities vary with the electron flux, we seek a metric that collapses the electron energy spectra into a single number. To obtain this metric we summed the SWEA electron energy spectra at each time over all energies greater than 13.6 eV, which is close to the ionization potentials of both CO_2 (13.77 eV) and O (13.62 eV) *[Schunk and Nagy*, 2009]. We call this metric the “ionizing electron flux” because it is a proxy for the total electron flux that can ionize CO_2 and O. Figure 3 shows the CO_2^+, O^+, O_2^+, and NO^+ ion densities at 160 (±2.5) km as a function the ionizing electron flux.

The CO_2^+ and O^+ densities increase with increasing ionizing electron flux, with the median CO_2^+ and O+ densities increasing by a factor of ~30. This strong dependence between CO+ and the electron flux is due to electron impact ionization of carbon dioxide, which is the most abundant neutral in the thermosphere *[Haider*, 1997; *Fillingim et al.,* 2007]. For O^+, the strong dependence is due to electron impact ionization of atomic oxygen as well as the reaction $CO_2{}^+ + O \rightarrow O^+ + CO_2$, which converts impact-produced CO_2^+ into O^+ *[Haider*, 1997].

The O_2^+ and NO^+ densities also increase with increasing ionizing electron flux, but the correlation is weaker. As the ionizing electron flux increases, the median O_2^+ density increases by a factor of ~10 while the median NO^+ density increases only by a factor of ~2. This weaker correlation can be explained by considering that O_2^+ and NO^+ are not produced directly by electron impact ionization because their parent neutrals, O_2 and NO, are only minor species in the thermosphere [*Fox*, 1993; *Bougher et al.,* 2015; *Mahaffy et al.,* 2015b]. Instead, these ions are produced by ion-neutral reactions that convert CO+ and O+ into O+ and NO+ *[Haider*, 1997; *Girazian et al.,* 2017]. Since these ion-neutral reactions are rapid, CO+ and O+ have short chemical lifetimes.

By contrast, the chemical lifetimes of O_2^+ and NO^+ are much longer because they are destroyed entirely (NO^+) or partially (O_2^+) through dissociative recombination *[González-Galindo et al.,* 2013; *Chaufray et al.,* 2014]. Some of the O_2^+ is also converted into NO^+ through ion-neutral reactions with N and NO. Furthermore, as the electron and ion densities become smaller in the absence of electron impact ionization, the chemical lifetimes of O_2^+

and NO^+ increase. As a consequence of their long chemical lifetimes, O_2^+ and NO^+ decay at a slower rate than CO_2+ and O^+, making them stable, and less dependent on the electron impact ionization rate.

3.3. Vertical Structure

To show how electron impact ionization affects the vertical structure of nightside ionosphere, we have constructed median ion altitude profiles during times of "low" and "high" ionizing electron flux. We chose the cutoff between low and high ionizing electron flux to be 10^6 eV/cm^2/s/sr based on visual inspection of the data (see Fig. 3). After grouping the ion densities by low and high ionizing electron flux, we separated the ion densities into 7 km altitude bins and found the median density within each bin. The median altitude profiles are shown in Figure 4.

As Figure 4 shows, the effects of electron impact ionization are most significant at altitudes below 200 km where precipitating electrons deposit most of their energy *[Fox et al.,* 1993; *Fillingim et al.,* 2007; *Lillis et al.,* 2009, 2011; *Haider et al.,* 2013]. In particular, the CO_2^+, O_2^+, and O^+ densities below 200 km are significantly increased during times of high ionizing electron flux. Furthermore, when the ionizing electron flux is high, there are distinct peaks in the CO_2^+, O_2^+, and O^+ profiles. When the ionizing electron flux is low, however, the O^+ peak is less distinct and the CO_2^+ and O_2^+ peaks are absent. The altitudes of the CO_2^+ and O_2^+ peaks are between 150–160 km, which is consistent with predictions of electron precipitation models [Fox *et al.,* 1993; *Haider*, 1997; *Fillingim et al.,* 2007; *Lillis et al.,* 2009, 2011; *Haider et al.,* 2013]. It should be noted, however,that a detailed comparison between the observed and predicted peak altitudes cannot be performed because the underlying neutral atmospheres used in the models, which are all different, may also be different than the underlying neutral atmosphere during the MAVEN observations. Nevertheless, the CO_2^+ and O_2^+ peak altitudes are broadly consistent with the model predictions.

Both NO^+ profiles lack a peak, and the NO^+ density increases with decreasing altitude down to at least 130 km. The NO^+ peak must be below 130 km, which is lower than the periapsis of MAVEN and thus cannot be observed by the NGIMS instrument. The weak dependence of NO^+ on the electron flux is, once again, a consequence of its long chemical lifetime, which is several hours at night *[Girazian et al.,* 2017]. With such a long chemical lifetime, NO^+ densities rarely decay to small values, so increases in the electron impact ionization rate only cause modest increases in the NO^+ density.

3.4. Influence of Crustal Magnetic Fields

Figure 5A shows the ionizing electron flux at 160 km as a function of magnetic field strength and magnetic elevation angle. The elevation angle is defined as $—\sin^{-1}(B_r/|B|)—$ where B_r is the radial component of the field and —B— is the magnitude of the field. An elevation angle of 0° indicates a strictly horizontal field orientation while an elevation angle of 90° indicates a strictly radial field orientation (cusp).

In weak crustal field regions (< 40 nT) the ionizing electron flux varies by several orders of magnitude and has a somewhat bifurcated distribution such that the flux is either low (~10^5 eV/cm^2/s/sr) or high (>10^7 eV/cm^2/s/sr). Alternatively, in strong crustal field regions the ionizing electron flux is almost always low, rarely exceeding 10^6 eV/cm^2/s/sr. This is the effect of strong horizontal crustal fields shielding the atmosphere from precipitating electrons *[Lillis and Brain*, 2013]. There are a few instances when the ionizing electron flux is high in strong crustal field regions, but these only occur when the magnetic field has a significant radial component such that the magnetic elevation angle is greater than 45°. These field lines can connect to the solar wind allowing for electrons to precipitate into the nightside thermosphere *[Mitchell et al.,* 2001; *Brain et al.,* 2007; *Lillis and Brain*, 2013].

To illustrate how nightside ion densities are influenced by crustal magnetic fields, Fig 5B-E shows the CO_2^+, O^+, O_2^+, and NO^+ densities at 160 km as a function of magnetic field strength. In these panels the colors indicate the level of the ionizing electron flux as shown in Panel A. Although there is considerable scatter in the ion data, the overall patterns of the CO_2^+ and O+ densities as a function of magnetic field strength (Panels B and C) are similar to the pattern of the ionizing electron flux (Panel A). That is, in weak crustal field regions the CO_2^+ and O^+ densities vary by nearly two orders of magnitude and are larger when the ionizing electron flux is high. In strong crustal field regions, however, the ion densities are almost always small, rarely exceeding 1 cm^{-3} except for the few cases when the ionizing electron flux is high in magnetic cusp regions. For magnetic field strengths less than 100 nT, the median CO_2^+ density is 3.0 cm^{-3} and the median O^+ density is 2.4 cm^{-3}. For magnetic field strengths exceeding 100 nT, the median CO_2^+ and O^+ densities are only 0.4 cm^{-3}.

The O_2^+ density (Panel D) also decreases with magnetic field strength. For field strengths less than 100 nT, the median O_2^+ density is 4.3 cm^{-3}, but for field strengths greater than 100 nT the median O_2^+ density is only 1.2 cm^{-3}.

The NO^+ (Panel E) density is only weakly dependent on the magnetic field strength. Because of this weak dependence, NO^+ becomes relatively more abundant in regions of strong crustal field. This is highlighted in Fig. 5F, which shows that the NO^+/O^+ ratio increases with increasing magnetic field strength. For magnetic field strengths less than 100 nT, the median NO^+/O^+ ratio is ~0.29, which is typical for the nightside ionosphere *[Girazian et al.,* 2017]. For magnetic field strengths greater than 100 nT, the median NO^+/O^+ ratio increases to 0.96.

The increased NO^+/O^+ ratio is a consequence of strong, horizontal crustal fields shielding the nightside atmosphere from precipitating electrons. Without electron impact ionization, nightside ions are not replenished as they decay. Since some of the O^+ decays into NO^+ through ion-neutral reactions with N and NO *[Haider*, 1997; *González-Galindo et a.,*2013], the NO^+/O_2^+ ratio increase over time, causing closed crustal field regions to have a higher fraction of NO^+ than surrounding areas.

4. Discussion and Conclusions

We have used MAVEN observations to show how ion densities in the nightside ionosphere of Mars vary with superthermal electron fluxes. We found that, below 200 km, CO_2^+ and O^+ densities increase with increasing electron flux. The higher densities are produced by electron impact ionization of CO_2 and O, and an ion-neutral reaction in which atomic oxygen converts impact-produced CO_2^+ into O^+ *[Haider*, 1997; *Fillingim et al.,* 2007]. The O_2^+ density below 200 km also increases with increasing electron flux, but to a lesser extent than CO_2^+ or O^+. Furthermore, the NO^+ density is only weakly dependent on the electron flux because NO^+ has a long chemical lifetime. Consequently, NO^+ densities are more stable and less sensitive to increases in the electron impact ionization rate.

High electron fluxes also produce distinct peaks of increased ion density in the CO_2^+, O^+, and O_2^+ altitude profiles. The altitudes of the CO_2^+ and O_2^+ peaks, between 150–160 km, are consistent with predictions of electron precipitation models [*Fox et al.,* 1993; *Haider*, 1997; *Fillingim et al.,* 2007, 2010; *Lillis et al.,* 2009, 2011; *Haider et al.,* 2013]. The NO^+ profile, however, lacks a distinct peak, even when electron fluxes are high. This is in stark contrast to electron precipitation models, which predict an NO^+ peak between 120–200 km [*Fox et al.,* 1993; *Haider*, 1997; *Haider et al.,* 2013]. The NO^+ peak must be below the periapsis of MAVEN where it cannot be observed in situ by the NGIMS instrument.

We have also shown that nightside ion densities are smaller near strong, horizontal crustal magnetic fields. These fields, which often form closed loops, act as an obstacle that prevents precipitating electrons from penetrating deep into the atmosphere [*Mitchell et al.,* 2001; *Brain et al.,* 2007; *Lillis and Brain*, 2013; *Steckiewicz et al.,* 2017]. Ions within these closed field regions decay without being replenished by electron impact ionization, which results in smaller ion densities. Additionally, because O_2^+ partially decays into NO^+ through ion-neutral reactions with N and NO, the NO^+/O_2^+ ratio is larger near strong, horizontal crustal fields. This ratio can even exceed unity at an altitude of 160 km so that NO^+ is the most abundant ion. These results complement previous studies which have found that the electron density and total electron content have a similar dependence on the strength and orientation of crustal magnetic fields [*Safaeinili et al.,* 2007; *Gurnett et al.,* 2008; *Němec et al.,* 2010, 2011; *Diéval et al.,* 2014; *Dubinin et al.,* 2016].

Although electron impact ionization is undoubtedly an important source of the nightside ionosphere, transport of ions from the dayside is also thought to be an important source near the terminator [Cui *et al.,* 2009; *González-Galindo et al.,* 2013; *Chaufray et al.,* 2014; *Ma et al.,* 2015]. Our results suggest that, when superthermal electrons are present, electron impact ionization is a significant source of CO_2^+ and O^+ below 200 km. This conclusion is supported by Fig. 4, which shows that when the electron flux is high, the median CO_2^+ and O^+ densities

below 200 km are increased by a factor of ~10. When the electron flux is low, however, CO_2^+ and O^+ decay rapidly leading to small nightside densities below 200 km.

In conclusion, electron impact ionization alters the chemical composition and vertical structure of the nightside ionosphere of Mars below 200 km. Future analyses of MAVEN data will be useful for understanding how, and when, superthermal electrons gain access to the nightside atmosphere. This may depend on upstream solar wind conditions [e.g., *Lillis and Brain*, 2013; *Diéval et al.,* 2014], which suggests that the solar wind dynamic pressure, and the orientation of the interplanetary magnetic field, will have a direct influence on the vertical structure and chemical composition of the nightside ionosphere of Mars.

Keypoints

- We show how superthermal electron fluxes and crustal magnetic fields affect ion densities in the nightside ionosphere of Mars.
- High electron fluxes increase nightside CO_2^+, O^+, and $O2^+$ densities below 200 km.
- Ion densities are smaller and the fractional abundance of NO^+ is larger near strong crustal magnetic fields.

Acknowledgments

Z.G.'s research was supported by an appointment to the NASA Postdoctoral Program at the NASA Goddard Space Flight Center, administered by Universities Space Research Association under contract with NASA. Z.G. thanks Joe Gre-bowsky, Yingjuan Ma, Janet Luhmann, Paul Withers, and Marissa Vogt for useful insights. The authors thank Jane Fox and an anonymous reviewer for their helpful suggestions. The data used in this publication are publicly available and can be downloaded from the the MAVEN Science Data Center (https://lasp.colorado.edu/maven/sdc/public/).

References

Benna M, Mahaffy PR, Grebowsky JM, Plane JMC, Yelle RV, Jakosky BM. Metallic ions in the upper atmosphere of Mars from the passage of comet C/2013 A1 (Siding Spring). Geophys. Res. Lett. 2015a; 42:4670–4675. . DOI: 10.1002/2015GL064159

Benna M, Mahaffy PR, Grebowsky JM, Fox JL, Yelle RV, Jakosky BM. First measurements of composition and dynamics of the Martian ionosphere by MAVEN's Neutral Gas and Ion Mass Spectrometer. Geophys. Res. Lett. 2015b; 42:8958–8965. . DOI: 10.1002/2015GL066146

Bougher SW, Pawlowski D, Bell JM, Nelli S, McDunn T, Murphy JR, Chizek M, Ridley A. Mars Global Ionosphere-Thermosphere Model: Solar cycle, seasonal, and diurnal variations of the Mars upper atmosphere. J. Geophys. Res. 2015; 120:311–342. . DOI: 10.1002/2014JE004715

Brain DA, Lillis RJ, Mitchell DL, Halekas JS, Lin RP. Electron pitch angle distributions as indicators of magnetic field topology near mars. J. Geophys. Res. 2007; 112:A09201. . doi: 10.1029/2007JA012435

Chaufray J-Y, Gonzalez-Galindo F, Forget F, Lopez-Valverde M, Leblanc F, Modolo R, Hess S, Yagi M, Blelly P-L, Witasse O. Three-dimensional Martian ionosphere model: II. Effect of transport processes due to pressure gradients. J. Geophys. Res. 2014; 119:1614–1636. . DOI: 10.1002/2013JE004551

Connerney JEP, Espley J, Lawton P, Murphy S, Odom J, Oliversen R, Sheppard D. The MAVEN Magnetic Field Investigation. Space Sci. Rev. 2015a; 195:257–291. . DOI: 10.1007/s11214-015-0169-4

Connerney JEP, Espley JR, DiBraccio GA, Gruesbeck JR, Oliversen RJ, Mitchell DL, Halekas J, Mazelle C, Brain D, Jakosky BM. First results of the MAVEN magnetic field investigation. Geophys. Res. Lett. 2015b; 42:8819–8827. . DOI: 10.1002/2015GL065366

Cui J, Galand M, Yelle RV, Vuitton V, Wahlund J-E, Lavvas PP, Müller-Wodarg ICF, Cravens TE, Kasprzak WT, Waite JH. Diurnal variations of Titan's ionosphere. J. Geophys. Res. 2009; 114:A06310. . doi: 10.1029/2009JA014228

Diéval C, Morgan DD, Němec F, Gurnett DA. MARSIS observations of the Martian nightside ionosphere dependence on solar wind conditions. J. Geophys. Res. 2014; 119:4077–4093. . DOI: 10.1002/2014JA019788

Dubinin E, Fraenz M, A. D, M. D. Martian Ionosphere observed by Mars Express. 1. Influence of the crustal magnetic fields. Planet. Space Sci. 2016; 124:62–75. . DOI: 10.1016/j.pss.2016.02.004

Fillingim MO, Peticolas LM, Lillis RJ, Brain DA, Halekas JS, Mitchell DL, Lin RP, Lummerzheim D, Bougher SW, Kirchner DL. Model calculations of electron precipitation induced ionization patches on the nightside of Mars. Geophys. Res. Lett. 2007; 34:L12101. . doi: 10.1029/2007GL029986

Fillingim MO, Peticolas LM, Lillis RJ, Brain DA, Halekas JS, Lummerzheim D, Bougher SW. Localized ionization patches in the nighttime ionosphere of Mars and their electrodynamic consequences. Icarus. 2010; 206:112–119. . DOI: 10.1016/j.icarus.2009.03.005

Fowler CM, Andersson L, Ergun RE, Morooka M, Delory G, Andrews DJ, Lillis RJ, McEnulty T, Weber TD, Chamandy TM, Eriksson AI, Mitchell DL, Mazelle C, Jakosky BM. The first in situ electron temperature and density measurements of the Martian nightside ionosphere. Geophys. Res. Lett. 2015; 42:8854–8861. . DOI: 10.1002/2015GL065267

Fox JL. The production and escape of nitrogen atoms on Mars. J. Geophys, Res. 1993; 98:3297–3310. . DOI: 10.1029/92JE02289

Fox JL, Brannon JF, Porter HS. Upper limits to the nightside ionosphere of mars. Geophys. Res. Lett. 1993; 20:1339–1342. . DOI: 10.1029/93GL01349

Girazian Z, Mahaffy PR, Lillis RJ, Benna M, Elrod M, Jakosky BM. Nightside ionosphere of Mars: Composition, vertical structure, and variability. J. Geophys. Res. 2017; 122:4712–4725. . DOI: 10.1002/2016JA023508

González-Galindo F, Chaufray J-Y, López-Valverde MA, Gilli G, Forget F, Leblanc F, Modolo R, Hess S, Yagi M. Three-dimensional Martian ionosphere model: I. The photochemical ionosphere below 180 km. J. Geophys. Res. 2013; 118:2105–2123. . DOI: 10.1002/jgre.20150

Gurnett DA, Huff RL, Morgan DD, Persoon AM, Averkamp TF, Kirchner DL, Duru F, Akalin F, Kopf AJ, Nielsen E, Safaeinili A, Plaut JJ, Picardi G. An overview of radar soundings of the martian ionosphere from the Mars Express spacecraft. Adv. Space Res. 2008; 41:1335–1346. . DOI: 10.1016/j.asr.2007.01.062

Haider SA. Chemistry of the nightside ionosphere of Mars. J. Geophys. Res. 1997; 102:407–416. . DOI: 10.1029/96JA02353

Haider SA, Kim J, Nagy AF, Keller CN, Verigin MI, Gringauz KI, Shutte NM, Szego K, Kiraly P. Calculated ionization rates, ion densities, and airglow emission rates due to precipitating electrons in the nightside ionosphere of Mars. J.G*eophys. Res.*. 1992; 97:10. . doi: 10.1029/92JA00317

Haider SA, Pandya BM, Molina-Cuberos GJ. Nighttime ionosphere caused by meteoroid ablation and solar wind electron-proton-hydrogen impact on Mars: MEX observation and modeling. J. Geophys. Res. 2013; 118:6786–6794. . DOI: 10.1002/jgra.50590

Jakosky BM, Lin RP, Grebowsky JM, Luhmann JG, Mitchell DF, Beutelshies G, Priser T, Acuna M, Andersson L, Baird D, Baker D, Bartlett R, Benna M, Bougher S, Brain D, Carson D, Cauffman S, Chamberlin P, Chaufray J-Y, Cheatom O, Clarke J, Connerney J, Cravens T, Curtis D, Delory G, Demcak S, DeWolfe A, Eparvier F, Ergun R, Eriksson A, Espley J, Fang X, Folta D, Fox J, Gomez-Rosa C, Habenicht S, Halekas J, Holsclaw G, Houghton M, Howard R, Jarosz M, Jedrich N, Johnson M, Kasprzak W, Kelley M, King T, Lankton M, Larson D, Leblanc F, Lefevre F, Lillis R, Mahaffy P, Mazelle C, McClintock W, McFadden J, Mitchell DL, Montmessin F, Morrissey J, Peterson W, Possel W, Sauvaud J-A, Schneider N, Sidney W, Sparacino S, Stewart AIF, Tolson R, Tou- blanc D, Waters C, Woods T, Yelle R, Zurek R. The Mars Atmosphere and Volatile Evolution (MAVEN) Mission. Space Sci. Rev. 2015; . doi: 10.1007/s11214-015-0139-x

Jakosky BM, Grebowsky JM, Luhmann JG, Brain DA. Initial results from the MAVEN mission to Mars. Geophys. Res. Lett. 2015b; 42:8791–8802. . DOI: 10.1002/2015GL065271

Lillis RJ, Brain DA. Nightside electron precipitation at Mars: Geographic variability and dependence on solar wind conditions. J. Geophys. Res. 2013; 118:3546–3556. . DOI: 10.1002/jgra.50171

Lillis RJ, Fang X. Electron impact ionization in the Martian atmosphere: Interplay between scattering and crustal magnetic field effects. J. Geophys. Res. 2015; 120:1332–1345. . DOI: 10.1002/2015JE004841

Lillis RJ, Fillingim MO, Peticolas LM, Brain DA, Lin RP, Bougher SW. Nightside ionosphere of Mars: Modeling the effects of crustal magnetic fields and electron pitch angle distributions on electron impact ionization. J. Geophys. Res. 2009; 114:E11009. . doi: 10.1029/2009JE003379

Lillis RJ, Fillingim MO, Brain DA. Three-dimensional structure of the Martian nightside ionosphere: Predicted rates of impact ionization from Mars Global Surveyor magnetometer and electron reflectometer measurements of precipitating electrons. J. Geophys. Res. 2011; 116:A12317. . doi: 10.1029/2011JA016982

Ma YJ, Russell CT, Fang X, Dong Y, Nagy AF, Toth G, Halekas JS, Connerney JEP, Espley JR, Mahaffy PR, Benna M, McFadden JP, Mitchell DL, Jakosky BM. MHD model results of solar wind interaction with Mars and comparison with MAVEN plasma observations. Geophys. Res. Lett. 2015; 42:9113–9120. . DOI: 10.1002/2015GL065218

Mahaffy PR, Benna M, King T, Harpold DN, Arvey R, Barciniak M, Bendt M, Carrigan D, Errigo T, Holmes V, Johnson CS, Kellogg J, Kimvilakani P, Lefa- vor M, Hengemihle J, Jaeger F, Lyness E, Maurer J, Melak A, Noreiga F, Noriega M, Patel K, Prats B, Raaen E, Tan F, Weidner E, Gundersen C, Battel S, Block BP, Arnett K, Miller R, Cooper C, Edmonson C, Nolan JT. The Neutral Gas and Ion Mass Spectrometer on the Mars Atmosphere and Volatile Evolution Mission. Space. Sci. Rev. 2015a; 195:49–73. . DOI: 10.1007/s11214-014-0091-1

Mahaffy PR, Benna M, Elrod M, Yelle RV, Bougher SW, Stone SW, Jakosky BM. Structure and composition of the neutral upper atmosphere of Mars from the MAVEN NGIMS investigation. Geophys. Res. Lett. 2015b; 42:8951–8957. . DOI: 10.1002/2015GL065329 [PubMed: 27667873]

Mitchell DL, Lin RP, Mazelle C, Reme H, Cloutier PA, Connerney JEP, Acuna MH, Ness NF. Probing Mars' crustal magnetic field and ionosphere with the MGS Electron Reflectometer. J. Geophys. Res. 2001; 106(23):419–23. 428. . DOI: 10.1029/2000JE001435

Mitchell DL, Mazelle C, Sauvaud J-A, Thocaven J-J, Rouzaud J, Fedorov A, Rouger P, Toublanc D, Taylor E, Gordon D, Robinson M, Heavner S, Turin P, Diaz-Aguado M, Curtis DW, Lin RP, Jakosky BM. The MAVEN Solar Wind Electron Analyzer. Space Sci. Rev. 2016; 200:495–528. . DOI: 10.1007/s11214-015-0232-1

Morschhauser A, Lesur V, Grott M. A spherical harmonic model of the lithospheric magnetic field of Mars. J. Geophys. Res. 2014; 119:1162–1188. . DOI: 10.1002/2013JE004555

Nier AO, McElroy MB. Composition and structure of Mars' upper atmosphere — Results from the neutral mass spectrometers on Viking 1 and 2. J. Geophys. Res. 1977; 82:4341–4349. . DOI: 10.1029/JS082i028p04341

Němec F, Morgan DD, Gurnett DA, Duru F. Nightside ionosphere of Mars: Radar soundings by the Mars Express spacecraft. J. geophys. Res. 2010; 115:E12009. . doi: 10.1029/2010JE003663

Němec F, Morgan DD, Gurnett DA, Brain DA. Areas of enhanced ionization in the deep nightside ionosphere of Mars. J. Geophys. Res. 2011; 116:E06006. . doi: 10.1029/2011JE003804

Safaeinili A, Kofman W, Mouginot J, Gim Y, Herique A, Ivanov AB, Plaut JJ, Picardi G. Estimation of the total electron content of the martian ionosphere using radar sounder surface echoes. Geophys. Res. Lett. 2007; 34:L23204. . doi: 10.1029/2007GL032154

Schunk RW, , and Nagy AF. (2009), Ionospheres, second. ed., Cambridge University Press , New York

Shane AD, Xu S, Liemohn MW, Mitchell DL. Mars nightside electrons over strong crustal fields. J. Geophys. Res. 2016; 121:3808–3823. . DOI: 10.1002/2015JA021947

Steckiewicz M, Garnier P, Andre N, Mitchell DL, Andersson L, Penou E, Beth A, Fedorov A, Sauvaud J-A, Mazelle C, Brain DA, Espley JR, McFadden J, Halekas JS, Larson DE, Lillis RJ, Luhmann JG, Soobiah Y, Jakosky BM. Comparative study of the Martian suprathermal electron depletions based on Mars Global Surveyor, Mars Express, and Mars Atmosphere and Volatile EvolutioN mission observations. J. Geophys. Res. 2017; 122:857–873. . DOI: 10.1002/2016JA023205

Withers P, Fillingim MO, Lillis RJ, Häusler B, Hinson DP, Tyler GL, Pätzold M, Peter K, Tellmann S, Witasse O. Observations of the nightside ionosphere of Mars by the Mars Express Radio Science Experiment (MaRS). J. Geophys, Res. 2012; 117:A12307. . doi: 10.1029/2012JA018185

Zhang MHG, Luhmann JG, Kliore AJ. An observational study of the nightside ionospheres of Mars and Venus with radio occultation methods. *J. Geophys,* Res.. 1990; 95(17):095–17. 102. . DOI: 10.1029/JA095iAl0p17095

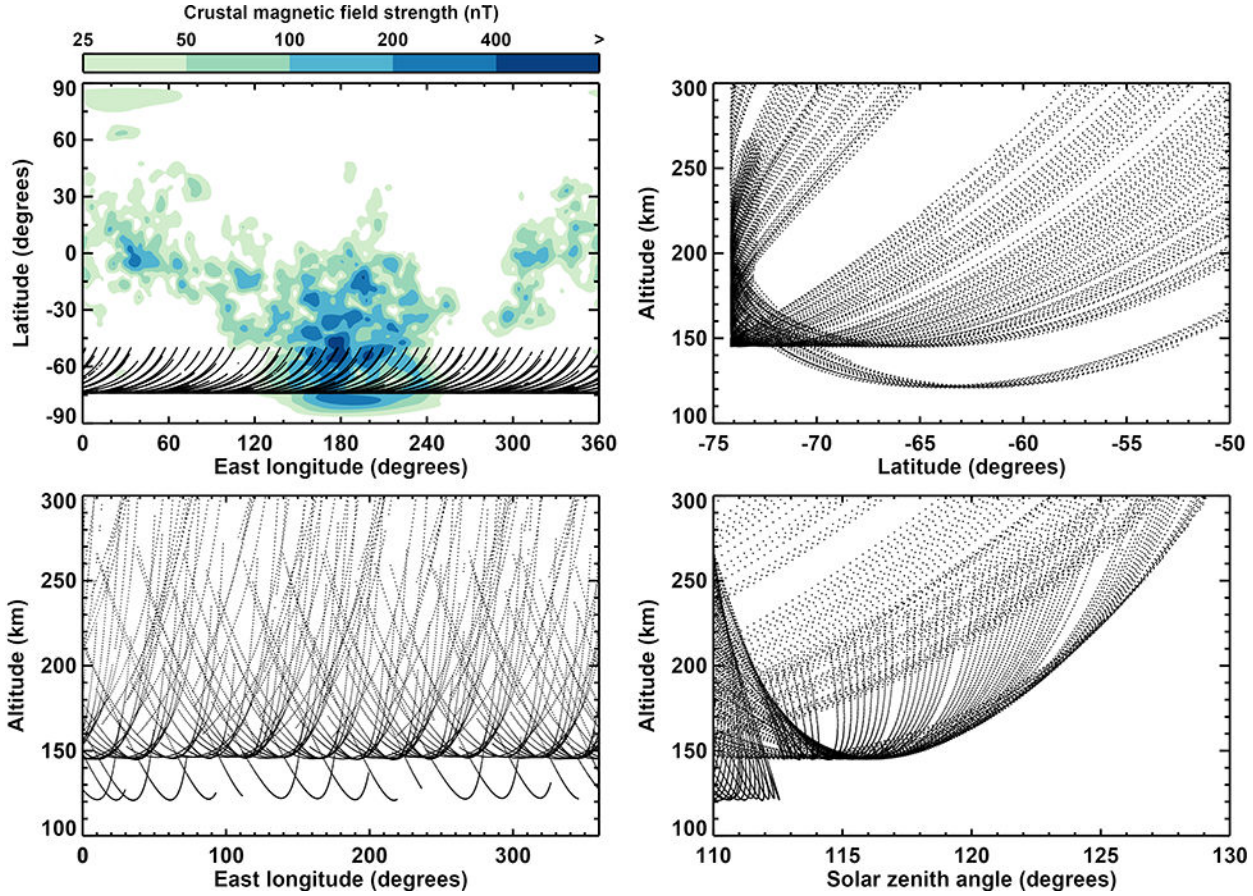

Figure 1.

Distribution of the nightside (SZA>110°) MAVEN observations used in this study. The top left panel shows the geographic distribution of the observations in relation to the crustal magnetic field strength at 200 km *[Morschhauser et al.,* 2014]. The remaining panels show the altitude distribution of the observations with respect to latitude, longitude, and solar zenith angle.

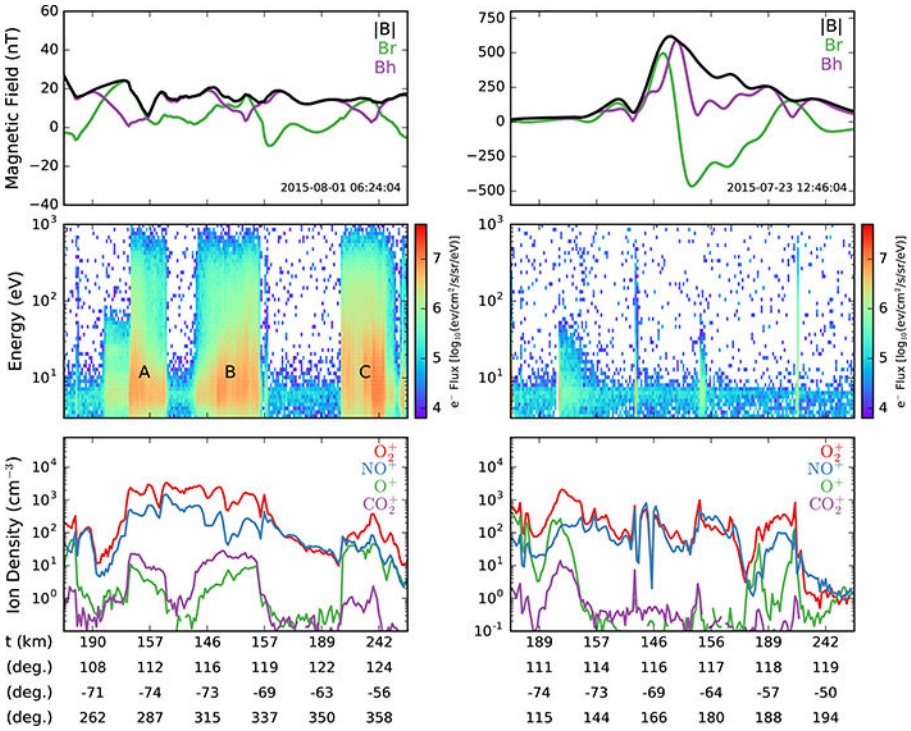

Figure 2.

Nightside measurements during two MAVEN periapsis passes. The left column shows a pass in a weak crustal field region and the right column shows a pass in a strong crustal field region. For each pass the top panel shows the MAG measurements of the total (—B—), radial (Br), and horizontal (Bh) components of the magnetic field, the middle panel shows the SWEA electron energy spectra, and the bottom panel shows the NGIMS ion densities. The A, B, and C labels in the left panel identify times of high SWEA electron fluxes during which the NGIMS CO_2^+ and O^+ densities increased significantly. By contrast, in the strong crustal field region shown in the right panel, high SWEA electron fluxes were only observed as narrow spikes in magnetic cusps where the field was predominately radial.

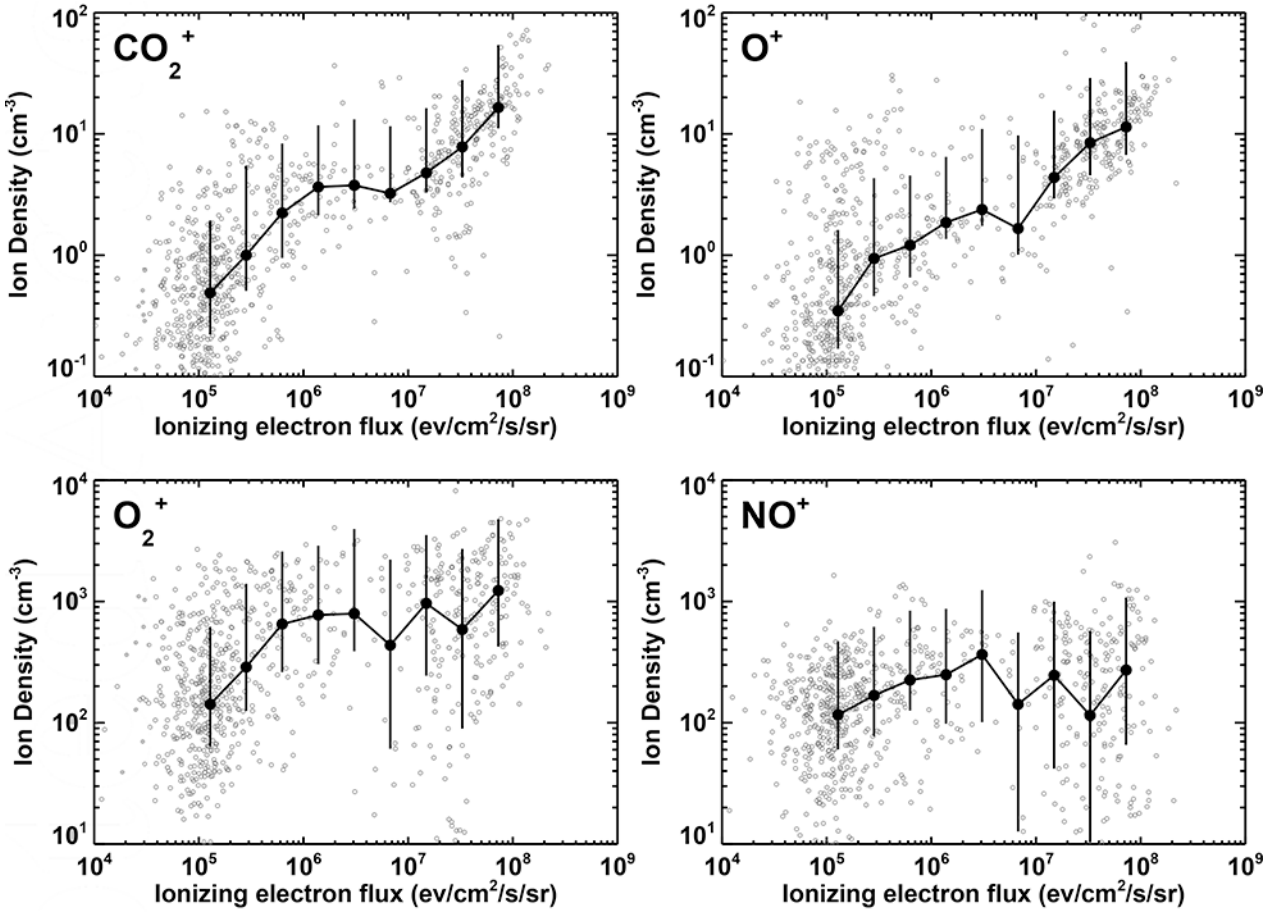

Figure 3.

Nightside ion densities at 160 km as a function of the ionizing electron flux. In each panel the gray circles show the NGIMS measurements, the black line shows a running median, and the error bars show the 25% and 75% quartiles. The scales of the ion density axes for CO_2^+ and O^+ are different than those for O_2^+ and NO^+.

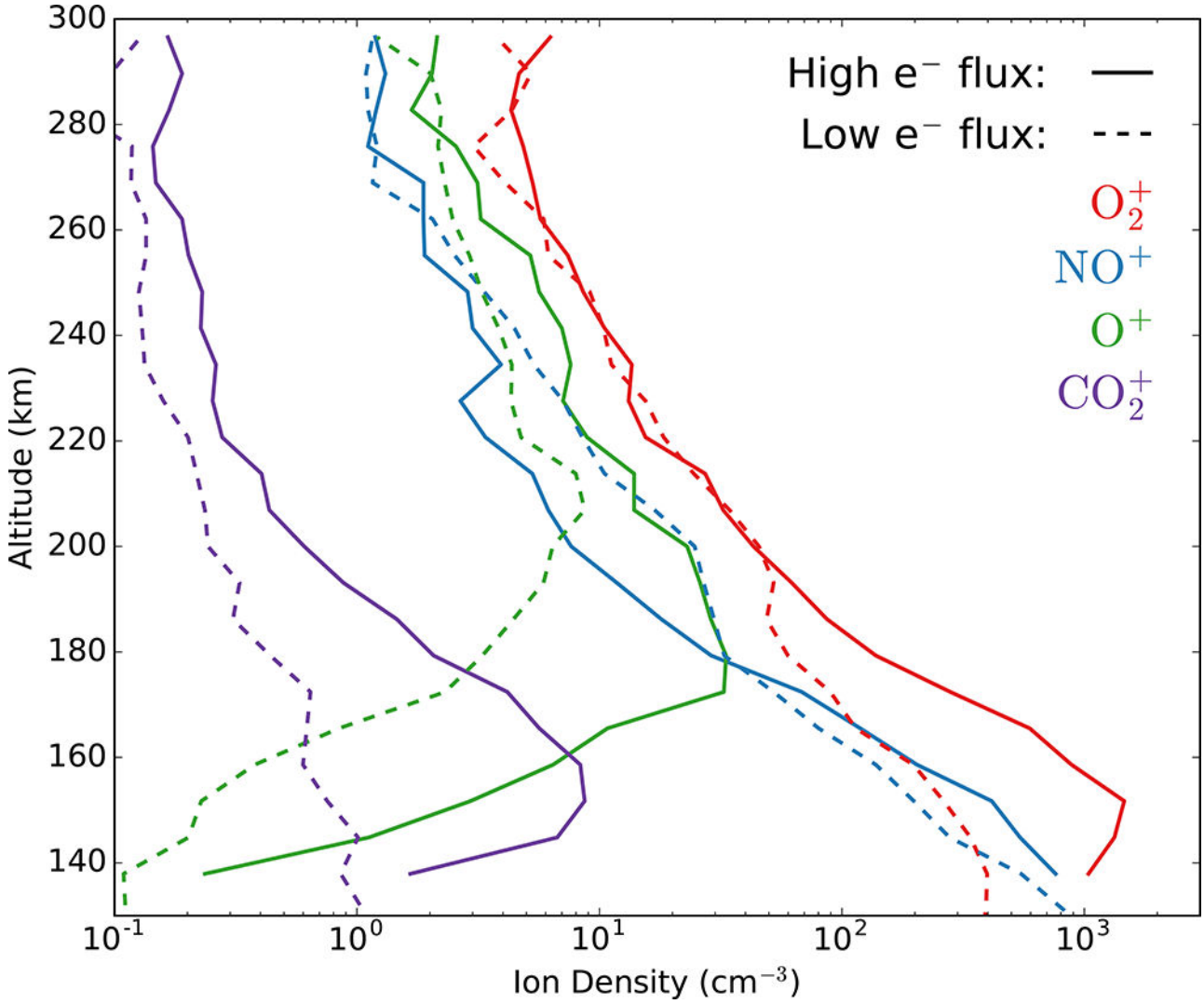

Figure 4.

Median altitude profiles of nightside O_2^+, NO^+, O^+, and CO_2^+ during times of low and high ionizing electron flux. The solid lines show median profiles for high ionizing electron flux (<10^6 eV/cm^2/s/sr) and the dashed lines show median profiles for low ionizing electron flux (<10^6 eV/cm^2/s/sr). The most significant effects of electron impact ionization are seen below 200 km, where distinct peaks in the O_2^+, O^+, and CO_2^+ profiles are present when the electron flux is high, but absent when the electron flux is low.

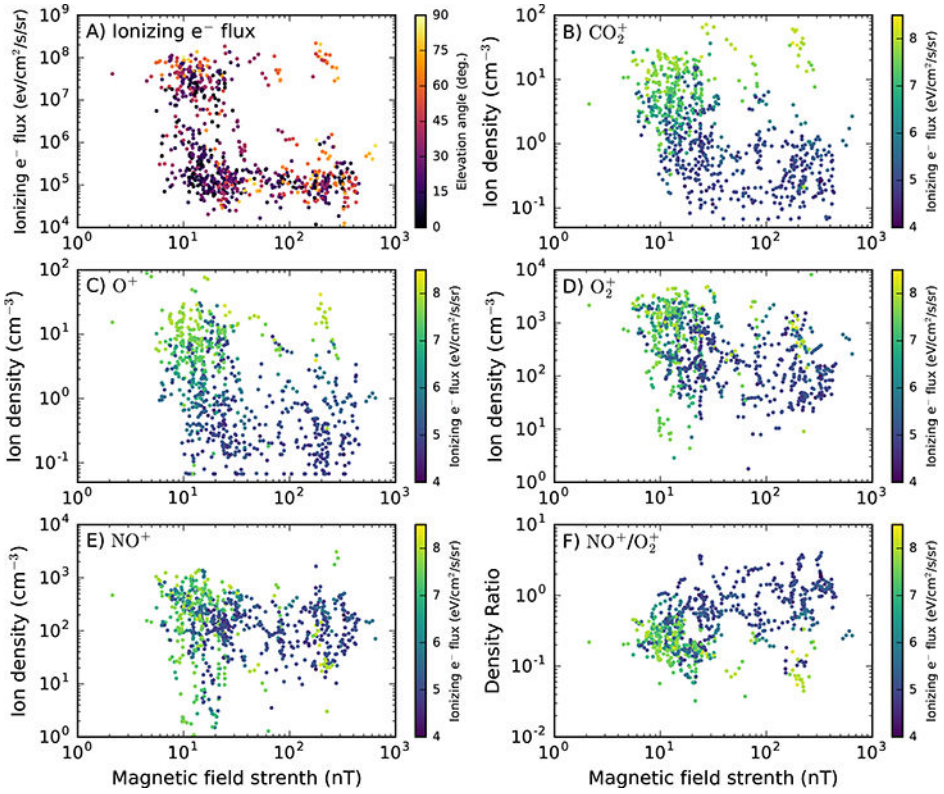

Figure 5.

A) The ionizing electron flux at 160 km as a function of magnetic field strength and evation angle. Ionizing electron fluxes are smaller in strong crustal field regions except for a few instances when the magnetic field has a significant radial component and the elevation angle exceeds 45°. **B-E)** Ion densities at 160 km as a function of magnetic field strength and the ionizing electron flux. The CO_2^+ and O^+ densities are significantly smaller in strong crustal field regions when the ionizing electron flux is low. The O_2^+ and NO^+ densities are also smaller in strong crustal field regions, but to a lesser extent. **F)** The NO^+/O_2^+ ratio as a function of magnetic field strength and ionizing electron flux. The ratio increases with magnetic field strength